CHEMISTRY OF MATERIALS
Article

Chem. Mater. **2009,** *21,* 3889–3897 3889
DOI:10.1021/cm9014223

A Systematic Study on Zinc Oxide Materials Containing Group I Metals (Li, Na, K)−Synthesis from Organometallic Precursors, Characterization, and Properties

S. Polarz,*[,†] A. Orlov,[†] A. Hoffmann,[‡] M. R. Wagner,[‡] C. Rauch,[‡] R. Kirste,[‡] W. Gehlhoff,[‡] Y. Aksu, M. Driess,[§] M. W. E. van den Berg,[⊥] and M. Lehmann[#]

[†]*Department for Chemistry, University of Konstanz, D-78457 Konstanz, Germany,* [‡]*Institute for Solid-State Physics, Technical University Berlin, Hardenbergstrasse 36, 10623 Berlin, Germany.,* [§]*Institute of Chemistry: Metalorganics and Inorganic Materials, Technical University Berlin, Sekr. C2, Straße des 17. Juni 135, 10623 Berlin, Germany,* [⊥]*Department for Chemistry, Ruhr-Universitaet Bochum, Universitaetsstrasse 150, 44780 Bochum, Germany, and* [#]*Institute for Optics and Atomic Physics, Technical University Berlin, Straße des 17. Juni 135, 10623 Berlin, Germany*

Received May 25, 2009

The reproducible preparation of p-type ZnO represents an important task that might be realized via the partial substitution of Zn^{2+} by Li^{+} in the ZnO lattice. Consequently, it is necessary to understand the effect of Li incorporation into ZnO in detail. A systematic approach employing molecular organometallic precursors for the preparation of ZnO materials containing different amounts of Li is presented. The materials have been characterized with various analytical techniques including X-ray absorption, micro-Raman, and low-temperature photoluminescence spectroscopy; high-resolution transmission electron microscopy; powder X-ray diffraction; and electron paramagnetic resonance. It could be seen that Li incorporation is successful only below 12% Li. Already at ∼1% Li, a maximum in lattice substitution seems to be reached. At higher Li contents, more and more interstitial sites become occupied.

1. Introduction

Wide band gap semiconductors are still receiving growing attention because of the wide spectrum of properties and applications.[1] Among them, zinc oxide (ZnO) is of extraordinary importance. It possesses a band gap of 3.37 eV,[2] and a rather high exciton binding energy of 60 meV which also allows lasing operation.[3] ZnO is a characteristic n-type semiconductor with piezoelectric and electromechanical coupling properties.[4] Furthermore, it was applied for UV light-emitting diodes, in photovoltaic solar cells, in UV photodetectors, for varistors, sensors, and even in heterogeneous catalysis.[5−8]

One of the major challenges in the field of ZnO materials is to establish a reliable method that can produce p-type ZnO in appreciable quantities, which is a difficult task because of the large binding energy of acceptor levels and the low solubility of acceptor dopants.[9] Promising candidates for shallow acceptor states are group I elements substituted for Zn^{2+} and the substitution of O^{2-} by group V elements. Because of shallow acceptor levels of alkali metals, Li^{+} seems to be predestinated.[9,10] It is characterized by the smallest binding energy of acceptor levels of reported dopants (0.09 eV)[9] and a high solubility in ZnO up to 30%.[11] One encountered problem is that Li can easily

*Corresponding author. Tel.: (+49)-7531-884415. Fax.: (+49)-7531-884406. E-mail: sebastian.polarz@uni-konstanz.de.

(1) (a) DeJule, R. *Semicond. Int.* **1999**, *22*, 34. (b) Henini, M. *Microelectron. J.* **1992**, *23*, 500. (c) Setaka, N. *Kagaku* (*Kyoto*) **1988**, *43*, 838.
(2) Kligshirn, C. *Phys. Status Solidi B* **1975**, *71*, 547.
(3) (a) *Landolt-Börnstein: Numerical Data and Functional Relationships in Science and Technology−New Series, Group III*; Springer-Verlag: Weinheim, Germany, 1999; Vol. *41B*.(b) Zu, P.; Tang, Z. K.;(b1) Wong, G. K. L.; Kawasaki, M.; Ohtomo, A.; Koinuma, H.; Segawa, Y. *Solid State Commun.* **1997**, *103*, 459. (c) Bagnall, D. M.; Chen, Y. F.; Zhu, Z.; Yao, T.; Koyama, S.; Shen, M. Y.; Goto, T. *Appl. Phys. Lett.* **1997**, *70*, 2230. (d) Tang, Z. K.; Wong, G. K. L.; Yu, P.; Kawasaki, M.; Ohtomo, A.; Koinuma, H.; Segawa, Y. *Appl. Phys. Lett.* **1998**, *72*, 3270.
(4) (a) Look, D. C. *Mater. Sci. Eng., B* **2001**, *80*, 383. (b) Hickerne, C. *IEEE Trans. Microwave Theory Tech.* **1969**, *MT17*, 957.
(5) Look, D. C.; Claftin, B. *Phys. Status Solidi B* **2004**, *241*, 624.
(6) (a) Meyer, B. K.; Alves, H.; Hofmann, D. M.; Kriegseis, W.; Forster, D.; Bertram, F.; Christen, J.; Hoffmann, A.; Strassburg, M.; Dworzak, M.; Haboeck, U.; Rodina, A. V. *Phys. Status Solidi B* **2004**, *241*, 231. (b) Martinez, M. A.; Herrero, J.; Gutierrez, M. T. *Solar Energy Mater. Solar Cells* **1997**, *45*, 75. (c) Anderson, N. A.; Ai, X.; Lian, T. Q. *J. Phys. Chem. B* **2003**, *107*, 14414. (d) Keis, K.; Lindgren, J.; Lindquist, S. E.; Hagfeldt, A. *Langmuir* **2000**, *16*, 4688. (e) Monroy, E.; Omnes, F.; Calle, F. *Semicond. Sci. Technol.* **2003**, *18*, R33. (f) Clarke, D. R. *J. Am. Ceram. Soc.* **1999**, *82*, 485. (g) Kung, H. H. *Catal. Rev. Sci. Eng.* **1980**, *22*, 235. (h) Klier, K. *Adv. Catal.* **1982**, *31*, 243. (i) Wilmer, H.; Kurtz, M.; Klementiev, K. V.; Tkachenko, O. P.; Grunert, W.; Hinrichsen, O.; Birkner, A.; Rabe, S.; Merz, K.; Driess, M.; Woell, C.; Muhler, M. *Phys. Chem. Chem. Phys.* **2003**, *5*, 4736.
(7) Polarz, S.; Roy, A.; Lehmann, M.; Driess, M.; Kruis, F. E.; Hoffmann, A.; Zimmer, P. *Adv. Funct. Mater.* **2007**, *17*, 1385.
(8) (a) Polarz, S.; Neues, F.; Van den Berg, M.; Grünert, W.; Khodeir, L. *J. Am. Chem. Soc.* **2005**, *127*, 12028. (b) Jana, S.; Aksu, Y.; Driess, M. *Dalton Trans.* **2009**, 1516.(c) Aksu, Y.; Jana S.; Driess, M.; Markus R. Wagner, M. R.; Kirste, R.;Callsen, G.; Gehlhoff, W.; Hoffmann A. Unpublished.
(9) Park, C. H.; Zhang, S. B.; Wei, S.-H. *Phys. Rev. B: Condens. Matter Mater. Phys.* **2002**, *66*, 073202/1.
(10) Wardle, M. G.; Goss, J. P.; Briddon, P. R. *Phys. Rev. B: Condens. Matter Mater. Phys.* **2005**, *71*, 155205/1.
(11) Joseph, M.; Tabata, H.; Kawai, T. *Appl. Phys. Lett.* **1999**, *74*, 2534.

Published on Web 08/04/2009

occupy interstitial positions in the lattice (Li_i) and then behaves as a shallow donor.[9,10] In addition, Li doping frequently results in the formation of semi-insulating, n-type ZnO materials.[5] Recently several reports about the successful preparation of p-type ZnO films using dc reactive magneton sputtering or pulsed laser deposition were published.[12,13] Two papers report a maximum in p-doping and extraordinary opto-electrical properties for lithium contents around 0.8 at % Li.[13,14] For higher Li contents, another interesting property of lithium-containing zinc oxide materials was reported: ferroelectricity.[15,16]

We were recently investigating a new molecular precursor system eligible for the preparation of various ZnO materials: organometallic zinc-oxo clusters of the general formula $[MeZnOR]_4$ containing a central "Zn_4O_4" core that can be transformed to ZnO either thermolytically or hydrolytically.[7,8,17−19] In the following, we will abbreviate the heterocubanes according to their respective inorganic core ($[MeZnOR]_4 \equiv$ "Zn_4O_4"). The substitution of zinc by alternative metals (Ni, Co, Mn, Fe) while maintaining the heterocubane core has been shown to increase the chemical complexity of the precursor.[20] It was demonstrated that the composition of the precursor determines the composition of the resulting material, precursors containing two different metals afford the respective bimetallic oxides.[20,21]

2. Experimental Section

Sample Preparation. *General Remarks*. All manipulations were carried out under anaerobic conditions using standard Schlenk techniques. Solvents were dried according to standard methods and distilled and degassed prior to use. All other chemical were of reagent grade and used without further purification.

Synthesis. *Compound "Zn_4O_4"*. The synthesis of $[MeZn-O^{tert}Bu]_4$ is described in a previous publication.[19]

Compound "Zn_3KO_4". The synthesis of $[Me_3Zn_3K(thf)-O^{tert}Bu_4]$ is described in a previous publication.[22]

Compound "Zn_3LiO_4". $[Me_3Zn_3K(thf)O^{tert}Bu_4]$ (3.9 g, 6.8 mmol) was dissolved in 20 mL of dry THF, mixed with 638 mg (6.8 mmol) of $LiBF_4$, and stirred for 2 h at rt. Volatile components were removed in vacuo (1×10^{-2} mbar), and the resulting white crude product was treated with CH_2Cl_2. After filtration, the clear colorless solution was evaporated, yielding 3.2 g (5.2 mmol, 77%) of a white powder. Single crystals were grown from CH_2Cl_2 at −20 °C.

^1H NMR (200 MHz, [D_6]benzene). δ −0.02 (s, 9H), 1.20−1.23 (m, 4H), 1.36 (s, 27H), 1.52 (s, 9H), 3.40−3.49 (m, 4H). ^{13}C NMR (50 MHz, [D_6]benzene): δ = −6.3, 25.1, 32.3, 33.1, 69.4, 70.8, 73.2.

Compound "Zn_3NaO_4". $[Me_3Zn_3K(thf)O^{tert}Bu_4]$ (4.4 g, 7.8 mmol) was dissolved in 60 mL of dry THF and mixed with a solution of 2.6 g (7.8 mmol) of $NaBPh_4$ in 30 mL of dry THF. After stirring for 4 h at rt, the suspension was filtered and the filtrate evaporated yielding 3.5 g (5.5 mmol, 71%) of a white powder. Single crystals were grown from CH_2Cl_2 at −20 °C.

^1H NMR (200 MHz, [D_6]benzene). δ −0.02 (s, 9H), 1.20−1.23 (m, 4H), 1.36 (s, 27H), 1.52 (s, 9H), 3.40−3.49 (m, 4H). ^{13}C NMR (50 MHz, [D_6]benzene): δ = −6.3, 25.1, 32.3, 33.1, 69.4, 70.8, 73.2.

Preparation of Powders. A certain amount of $[(CH_3)_3Zn_3Li-(THF)(OC(CH_3))_4]$ (see Table 2) was dissolved in carefully dried THF. Subsequently, a certain amount of $[CH_3ZnOC(CH_3)_3]_4$ is added (see Table 2). The solution is stirred until both compounds have dissolved completely. The THF is removed in oil-pump vacuum. The obtained white powder is transferred into a tube oven and heated for 3 h at 750 °C (heating rate 4 K per minute) in an atmosphere containing pure oxygen. The desired oxide powders are obtained in quantitative yield.

Analytical Techniques. IR spectra were performed on a Perkin-Elmer Spectrum 100 FT-IR spectrometer using a Perking Elmer Universal ATR sampling accessory. X-ray diffraction was performed on a Bruker AXS D8 Advance diffractometer using $Cu_{k\alpha 1}$ radiation and a Bruker AXS Sol-X solid state energy dispersive detector position. The UV/vis measurements were done on a Varian Cary 100 scan UV/vis spectrophotometer. The absorption coefficient was determined using the relation $\alpha(\lambda) = D^{-1} \ln [(1 - R(\lambda))^2/T(\lambda)]$ with $D \cong$ sample thickness, $R \cong$ reflectance, and $T \cong$ transmission. Band-gap energies (E_g) were acquired from a plot of ($\alpha \times E_{Photon}$) versus E_{Photon}.

TGA measurements were performed on a setup by Rubotherm. Elemental analysis on lithium was performed by an external laboratory (Institut Fresenius, Taunusstein, Germany). A sample mixture that was designated to yield a material containing 0.3 wt % Li, contained in reality 0.3035 wt %, a sample designated to yield a material containing 0.15 wt % Li, contained in reality 0.1600 wt %. XAS experiments were performed at beamline E4 (HASYLAB) at the Zn K-edge. The (atomic resolution) TEM images were recorded at the FEI Tecnai F20/Cs-corr TEM located at the Triebenberg Lab of the TU Dresden. This TEM is equipped with a field-emission electron source and operates at 200 kV acceleration voltage. The spherical aberration of the objective lens is corrected by means of a Cs-corrector, which allows the correction

(12) (a) Zeng, Y. J.; Ye, Z. Z.; Xu, W. Z.; Chen, L. L.; Li, D. Y.; Zhu, L. P.; Zhao, B. H.; Hu, X. L. *J. Cryst. Growth* **2005**, *283*, 180. (b) Zeng, Y. J.; Ye, Z. Z.; Xu, W. Z.; Li, D. Y.; Lu, J. G.; Zhu, L. P.; Zhao, B. H. *Appl. Phys. Lett*. **2006**, *88*, 062107/1. (c) Xiao, B.; Ye, Z.; Zhang, Y.; Zeng, Y.; Zhu, L.; Zhao, B. H. *Appl. Surf. Sci*. **2006**, *253*, 895. (d) Wang, X. H.; Yao, B.; Zhang, Z. Z.; Li, B. H.; Wei, Z. P.; Shen, D. Z.; Lu, Y. M.; Fan, X. W. *Semicond. Sci. Technol*. **2006**, *21*, 494.
(13) Lu, J. G.; Zhang, Y. Z.; Ye, Z. Z.; Zeng, Y. J.; He, H. P.; Zhu, L. P.; Huang, J. Y.; Wang, L.; Yuan, J.; Zhao, B. H.; Li, X. H. *Appl. Phys. Lett*. **2006**, *89*, 112113/1.
(14) Aghamalyan, N. R.; Goulanian, E. K.; Hovsepyan, R. K.; Vardanyan, E. S.; Zerrouk, A. F. *Phys. Status Solidi* **2003**, *199*, 425.
(15) (a) Onodera, A.; Tamaki, N.; Kawamura, Y.; Sawada, T.; Sakagami, N.; Jin, K.; Satoh, H.; Yamashita, H. *J. Korean Phys. Soc*. **1998**, *32*, S11. (b) Onodera, A.; Yoshio, K.; Satoh, H.; Takama, T.; Fujita, M.; Yamashita, H. *Ferroelectrics* **1999**, *230*, 465. (c) Tang, I. T.; Chen, H.-J.; Hwang, W. C.; Wang, Y. C.; Houng, M.-P.; Wang, Y.-H. *J. Cryst*. **2004**, *262*, 461.
(16) Islam, Q. T.; Bunker, B. A. *Phys. Rev. Lett*. **1987**, *59*, 2701.
(17) (a) Polarz, S.; Orlov, A.; Schüth, F.; Lu, A. H. *Chem.—Eur. J*. **2007**, *13*, 592. (b) Van den Berg, M.; Polarz, S.; Tkachenko, O. P.; Klementiev, K. V.; Bandyopadhyay, M.; Khodeir, L.; Gies, H.; Muhler, M.; Grünert, W. *J. Catal*. **2006**, *241*, 446. (c) Polarz, S.; Strunk, J.; Ischenko, V.; Van den Berg, M.; Hinrichsen, O.; Muhler, M.; Driess, M. *Angew. Chem*. **2006**, *118*, 3031. (d) Roy, A.; Polarz, S.; Merz, M.; Schneider, L.; Halm, S.; Bacher, G.; Kruis, F. E.; Driess, M. *Proc. Electrochem. Soc*. **2005**, *2005−09*, 537. (e) Schroeder, D.; Schwarz, H.; Polarz, S.; Driess, M. *Phys. Chem. Chem. Phys*. **2005**, *7*, 1049.
(18) Polarz, S.; Roy, A.; Merz, M.; Halm, S.; Schröder, D.; Scheider, L.; Bacher, G.; Kruis, F. E.; Driess, M. *Small* **2005**, *1*, 540.
(19) Ischenko, V.; Polarz, S.; Grote, D.; Stavarache, V.; Fink, K.; Driess, M. *Adv. Funct. Mater*. **2005**, *15*, 1945.
(20) Polarz, S.; Orlov, A.; Van den Berg, M.; Driess, M. *Angew. Chem., Int. Ed*. **2005**, *44*, 7892.
(21) (a) Orlov, A.; Roy, A.; Lehmann, M.; Driess, M.; Polarz, S. *J. Am. Chem. Soc*. **2007**, *129*, 371. (b) Roy, A.; Polarz, S.; Rabe, S.; Rellinghaus, B.; Zahres, H.; Kruis, F. E.; Driess, M. *Chem.—Eur. J*. **2004**, *10*, 1565.
(22) Merz, K.; Block, S.; Schoenen, R.; Driess, M. *Dalton Trans*. **2003**, 3365.

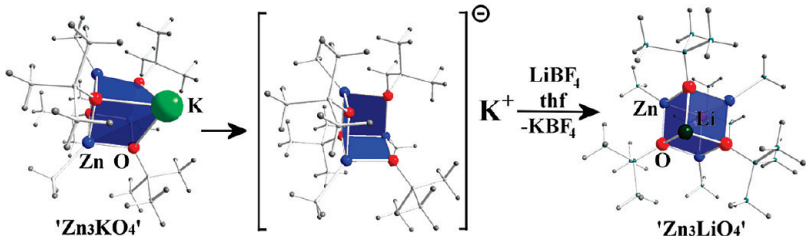

Figure 1. Molecular structure of $[Me_3Zn_3K(thf)O^{tert}Bu_4]$ determined by single-crystal X-ray diffraction,[22] the proposed transition state indicating the tridentate oxo-cluster ligand $[Me_3Zn_3O^{tert}Bu_4]$, and the resulting, new Li-containing, bimetallic heterocubane $[Me_3Zn_3Li(thf)O^{tert}Bu_4]$. The tetrahydrofurane (THF) molecules binding to the alkali metal have been omitted for reasons of clarity.

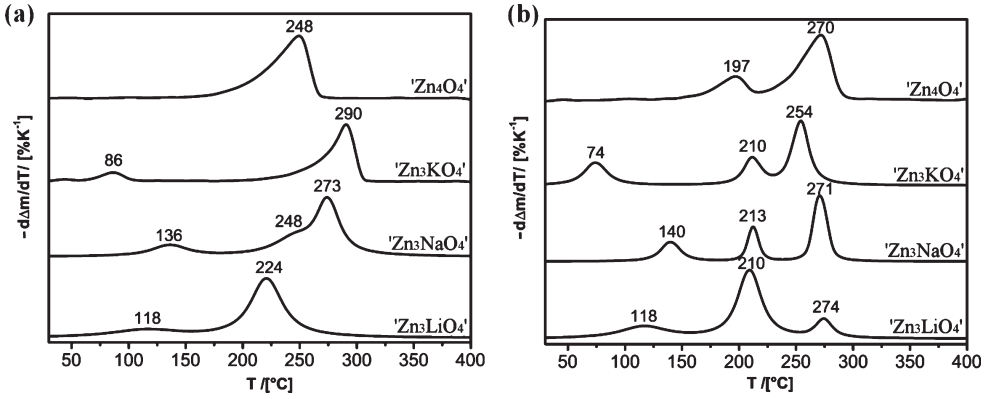

Figure 2. Thermochemical data (first-derivative traces of TGA measurements) for the heterocubane $[MeZnO^{tert}Bu]_4$ as a reference, $[Me_3Zn_3K(thf)O^{tert}Bu_4]$, $[Me_3Zn_3Li(thf)O^{tert}Bu_4]$, and $[Me_3Zn_3Na(thf)O^{tert}Bu_4]$. Measurements were performed under (a) nitrogen and (b) oxygen with a heating rate of 1 K/min.

of all coherent aberrations up to third order. As a consequence, bulk and surfaces of clusters are imaged without delocalization showing the true positions of atomic columns. The TEM samples were prepared by shortly dipping a Cu carrier covered with a holey carbon foil (Plano company, S147) in the solution consisting of dispersed Li−ZnO particles in acetone. From the atomically resolved TEM images, the diffractograms are determined by Fourier transformation of TEM image. PL measurements of the near-band-edge emission were performed using the 325 nm line of a HeCd laser. The emission was dispersed by a 0.8 m Spex double monochromator with a resolution better than 0.1 meV. A 9789QB bialkali photomultiplier tube was used to detect the emission. For measurements in the spectral region of the deep center emission, the 532 nm line of a frequency doubled Nd:YAG laser in combination with a GaAs PMT was used. NMR-spectra were acquired on a Bruker Avance DPX 250 spectrometer using dried C_6D_6 or $CDCl_3$ as a solvent. Solid-State NMR spectra were recorded using a Bruker DRX 400 spectrometer. SEM was measured using a Zeiss CrossBeam 1540XB instrument.

3. Results and Discussion

Considering the large interest in p-type doping of ZnO and in ferroelectric materials, it is a tempting goal to develop a precursor system that allows the preparation of alkali-metal doped ZnO materials, and especially Li-doped ZnO. Some time ago, the synthesis of a heterobimetallic cubane was reported where one zinc is substituted by potassium,[22] however, without probing this compound as a precursor for K-doped ZnO. The mentioned heterocubanes can be interpreted as a coordination compound between the anionic cluster fragment $[Me_3Zn_3(OR)_4]^-$ and a monocationic metal fragment $[ML]^+$ ($\cong {}^+$ZnMe, K) as indicated in Figure 1.[8a]

The potassium-containing compound "Zn_3KO_4" can be transformed into other interesting, bimetallic heterocubanes by metathesis reactions. For instance, the reaction of "Zn_3KO_4" with $LiBF_4$ in THF as a solvent yields $[Me_3Zn_3LiO^{tert}Bu_4] \equiv$ "Zn_3LiO_4" (see Experimental Section). In analogy, "Zn_3KO_4" can also be reacted with $NaBPh_4$ to give $[Me_3Zn_3Na(thf)O^{tert}Bu_4] \equiv$ "Zn_3NaO_4" (see the Supporting Information, SI-1). Moreover, Driess et al. have successfully developed a simple and efficient one-pot method to synthesize monolithium zinc alkoxo cubanes with a $[LiZn_3O_4]$ framework and different alkoxy and alkyl groups.[8b] Interestingly, the same synthetic strategy is even suitable for the preparation of analogues compounds containing Na, K, Rb, and Cs in high yield.[8c] Because the composition of the inorganic core of the mentioned compounds is "$Zn_3M_1O_4$" with M ≅ Li, Na, K it is interesting to investigate the potential as single-source precursors for the preparation of alkali-metal containing ZnO materials. The thermochemical properties of the pure heterobimetallic precursors "Zn_3MO_4" in comparison to the monometallic zinc-analogue $[MeZnO^{tert}Bu]_4 \equiv$ "Zn_4O_4" were studied using thermogravimetric analysis.

Qualitatively, the behavior of the compounds "Zn_3MO_4" and "Zn_4O_4" are similar with the difference that the THF molecule coordinating to the alkali metal is released at lower temperatures (see Figure 2). Assuming that the temperature where THF is released is indicative for the bond-strength of the oxygen-donor in thf and the alkali metal, it surprisingly seems that thf is bonded strongest to the sodium containing heterocubane (**3**) ($T_{thf\text{-}release}$ = 136 °C), followed by the lithium containing cubane (**2**)

($T_{\text{thf-release}}$ = 118 °C), followed by the potassium containing cubane (**1**) ($T_{\text{thf-release}}$ = 86 °C). Considering the boiling point of pure THF (T_{boiling} = 65 °C), it is bonded to potassium only weakly.

It has to be noted that the absence or presence of oxygen during the reaction of the precursors is of high relevance. The mass loss (see Table 1) under inert-gas conditions is much higher than expected for the transition from the precursor to the bimetallic oxide ("Zn_3MO_4" → MZn_3O_4). The difference between oxidative and nonoxidative treatment is most pronounced for "Zn_3LiO_4". The described observation can be explained if either significantly different products than the proposed oxides form, or if the precursors possess significant volatility similar to "Zn_4O_4" for which this has been proven already.[18] The latter assumption is supported by the fact that "Zn_3LiO_4" can be sublimated (see the Supporting Information, SI-2). The sublimation is much less pronounced in the presence of oxygen (Table 1). Therefore, an oxygen atmosphere was preferred for the synthesis of Li-containing ZnO materials. The corresponding TGA data shown in the Supporting Information, SI-3, revealed that in pure oxygen the remaining mass of 43.8% (Δm = −56.2%) fits very well to the theoretical value of Δm = −56.4% (see Table 1) expected for the full transformation of the "Zn_3LiO_4" precursor without unwanted evaporation.

Table 1. Comparison between the Experimentally Found And Theoretically Expected Values for Mass Loss

proposed reaction	N_2 Δm_{exp} (%)	20% O_2 Δm_{exp} (%)	Δm_{th} (%)
"Zn_3KO_4" → $4K_{0.25}Zn_{0.75}O$	−73.6	−51.2	−53.7
"Zn_3NaO_4" → $4Na_{0.25}Zn_{0.75}O$	−73.3	−49.6	−55.0
"Zn_3LiO_4" → $4Li_{0.25}Zn_{0.75}O$	−86.2	−68.9	−56.4

The powder X-ray diffraction (PXRD) patterns of the products obtained via oxidative treatment of "Zn_3KO_4", "Zn_3NaO_4", and "Zn_3LiO_4" are characterized by ZnO with wurtzite structure for all three samples (see Figure 3a−c). Because amorphous impurities will not be seen in PXRD, we also recorded FT-IR spectra. The spectra measured for the oxide materials originating from precursors "Zn_3NaO_4" and "Zn_3LiO_4" are shown in Figure 3d,e. The vibration at 450 cm^{-1} is characteristic for ZnO. However, the bands at 1400−1300 cm^{-1} indicate that also significant amounts of carbonates (CO_3^{2-}, HCO_3^-) and hydroxides (3390 cm^{-1}) are present. Elemental analyses of the samples shows that 10−15% of the alkali metals are present in the form of carbonates, and thus have not substituted Zn in the ZnO lattice as desired.

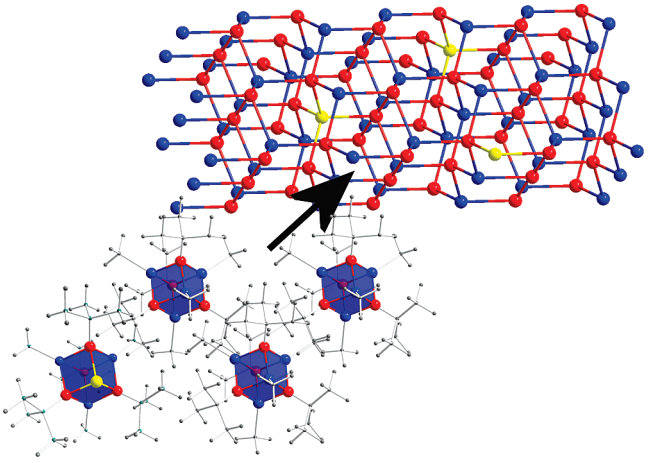

Figure 4. Powders of a cocrystal containing the organometallic heterocubanes [$Me_3ZnLi(O^{tert}Bu)_4$] and [$Me_4Zn_4(O^{tert}Bu)_4$] in different ratios have been used as the precursor for the synthesis of Li-doped ZnO materials. Zn ≡ blue; O ≡ red; Li ≡ yellow; C and H ≡ gray.

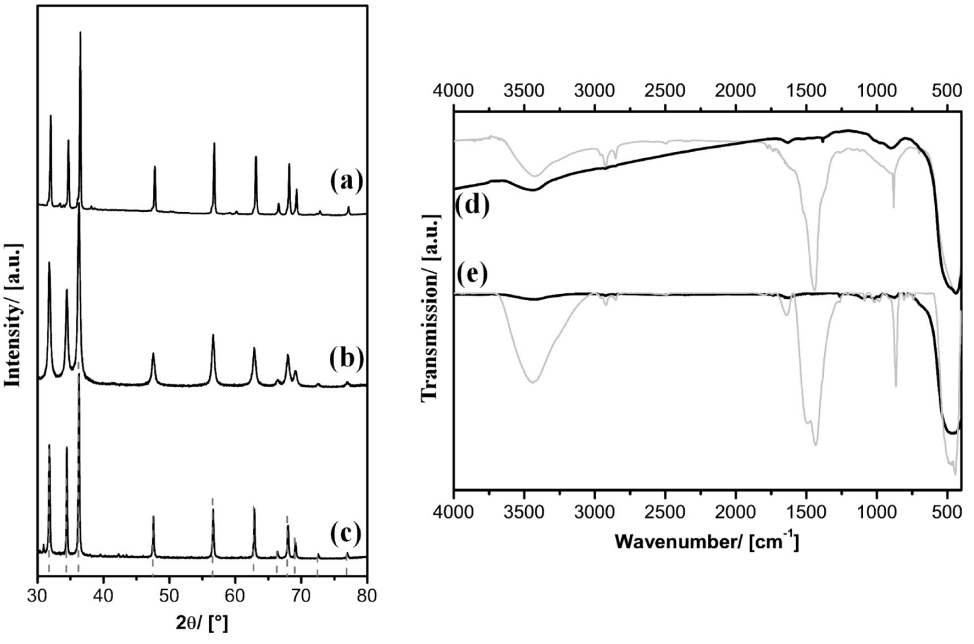

Figure 3. PXRD pattern of the products obtained from the decomposition of the precursors (a) "Zn_3LiO_4", (b) "Zn_3NaO_4", and (c) "Zn_3KO_4". The dashed gray lines indicate the diffraction pattern of pure ZnO as a reference. FT-IR spectra of the products obtained from the decomposition of the pure precursor at 750 °C in pure oxygen (gray) in comparison to a dilution of one part "Zn_3MO_4" with three parts "Zn_4O_4" (black curve): for (d) "Zn_3NaO_4" and (e) "Zn_3LiO_4".

Table 2. Precursor Mixtures to Obtain Li-Containing ZnO Powders

	precursor mixture		resulting oxide materials		
sample no.	m("Zn_4O_4") (g)	m("Zn_3LiO_4") (g)	designated formula	m(Li) (%)	at % Li
1	10	0.040	$Li_{0.001}Zn_{0.999}O$	0.0087	0.05
2	10	0.667	$Li_{0.015}Zn_{0.985}O$	0.14	0.75
3	10	1.429	$Li_{0.03}Zn_{0.97}O$	0.27	1.5
4	10	3.333	$Li_{0.06}Zn_{0.94}O$	0.57	3
5	10	5.544	$Li_{0.09}Zn_{0.91}O$	0.83	4.5
6	10	10	$Li_{0.12}Zn_{0.88}O$	1.2	6

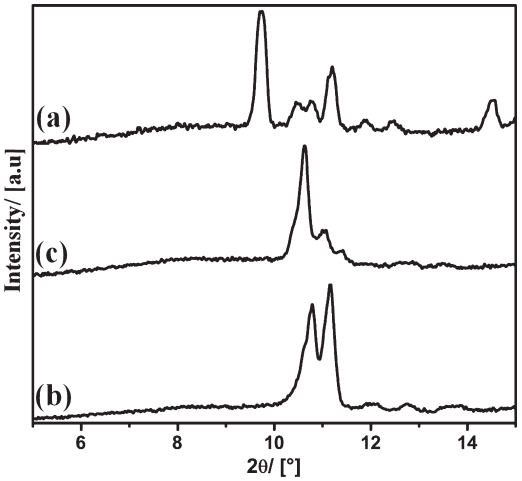

Figure 5. PXRD pattern of powders: (a) the precursor containing only zinc, $[MeZnO^{tert}Bu]_4$, in its pure form as a reference; (b) the precursor containing zinc and lithium ($[Me_3Zn_3Li(thf)O^{tert}Bu_4]$), as a reference; and (c) the precipitated 3:1 mixture of the latter compounds.

A possible explanation might be that the amount of for instance Li with respect to ZnO is too high and exceeds the solubility limit. If the latter hypothesis is correct, the problem might be overcome if the concentration of Li can be decreased, for instance, via molecular dilution of the precursor "Zn_3LiO_4" in a matrix of the precursor "Zn_4O_4" (Figure 4). Consequently, $[Me_3Zn_3Li(thf)O^{tert}Bu_4]$ and $[MeZnO^{tert}Bu]_4$ were dissolved in THF in different ratios (see the Experimental Section and Table 2).

After solvent removal, the precursor powders are obtained, which should enable the preparation of Li-containing zinc oxide materials $Li_xZn_{1-x}O$. A necessity for the proposed method is that the two different heterocubanes "Zn_3LiO_4" and "Zn_4O_4" form solid solutions in the solid state and do not form separate phases. Both precursors in their pure form give rise to distinct PXRD patterns (see Figure 5). The PXRD pattern of a 3:1 mixture is clearly not a superposition of the diffraction patterns of "Zn_4O_4" and "Zn_3LiO_4", indicating that the precursors form a molecular dispersion also in the crystalline state.

The 3:1 precursor mixture was treated at $T = 750$ °C in pure oxygen, and FT-IR spectra were recorded from the product (Figure 3e). The band characteristic for ZnO can be seen; however, the bands indicating the presence of carbonates are absent. It is worth noting that the described method works as well for the preparation of carbonate-free Na-containing ZnO materials (see Figure 3d). Elemental analysis performed on the Li containing samples shows that the Li: Zn content can be adjusted via the preparation of the appropriate precursor mixture. It is now possible to vary the amount of Li in the resulting oxide materials systematically. ZnO powders containing $Li_x:Zn_{1-x}$ (x = 25, 12, 6, 3, 1.5, 0.01%) have been prepared. The resulting metal oxides were analyzed by a variety of methods: PXRD, X-ray absorption spectroscopy (XAS), FT-IR spectroscopy, FT-Raman spectroscopy, solid-state nuclear magnetic resonance spectroscopy (ST-NMR), reflectance UV/vis spectroscopy, electron paramagnetic resonance spectroscopy (EPR), photoluminescence spectroscopy, scanning electron microscopy (SEM), and transmission electron microscopy (TEM).

The homogeneity of the samples was checked by SEM recorded in topography mode (see the Supporting Information, SI-4) and in backscattering electron mode (Figure 6a,b and the Supporting Information, SI-4). The images from backscattered electrons which are sensitive regarding composition indicate a homogeneous distribution in the samples with Li concentrations of $x = 0.01-12\%$. In the images recorded from the sample containing 25% Li light spots are seen all over the material, which is in agreement with the previous finding of an undesired lithium carbonate phase. The distribution, size, and crystallography were investigated by conventional TEM (Figure 6c) and atomic resolution TEM (Figure 6d; see also the Supporting Information, SI-5). For the sample with 1.5% Li in ZnO (Figure 6c), single particles with sizes ranging from 20 to 70 nm are conglomerated to larger ones. The corresponding atomically resolved TEM-micrograph shows the Wurtzite structure of ZnO with a high density of stacking faults. As it can be observed from the diffractograms, the Wurtzite structure becomes less ordered with increasing Li content (Figure 6d and the Supporting Information, SI-5).

The PXRD patterns of the samples (exemplarily shown for $x = 3\%$ and 12% in Figure 7a,b) contain only reflexes which can be assigned to ZnO with wurtzite structure. The entire diffractograms were evaluated using Warren-Averbach fits (see Figure 7a,b and the Supporting Information, SI-6). In comparison to the values reported for pure ZnO in the literature ($a = 324.8$ pm, $c = 520.3$ pm)[23] an expansion of lattice parameters was found for the Li-containing ZnO samples. Parameter c (≈ 523 pm for most samples) varies only weakly with varying Li content and parameter a more strongly (325.9−326.8 pm). According to our data, there is a maximum in the lattice parameter deviation between 1.5 and 3% Li content.

(23) Reeber, R. R. *J. Appl. Phys.* **1970**, *41*, 5063.
(24) Fallert, J.; Hauschild, R.; Stelzl, F.; Urban, A.; Wissinger, M.; Zhou, H. J.; Klingshirn, C.; Kalt, H. *J. Appl. Phys.* **2007**, 101.
(25) Zeng, Y. J.; Ye, Z. Z.; Lu, J. G.; Xu, W. Z.; Zhu, L. P.; Zhao, B. H.; Limpijumnong, S. *Appl. Phys. Lett.* **2006**, 89.

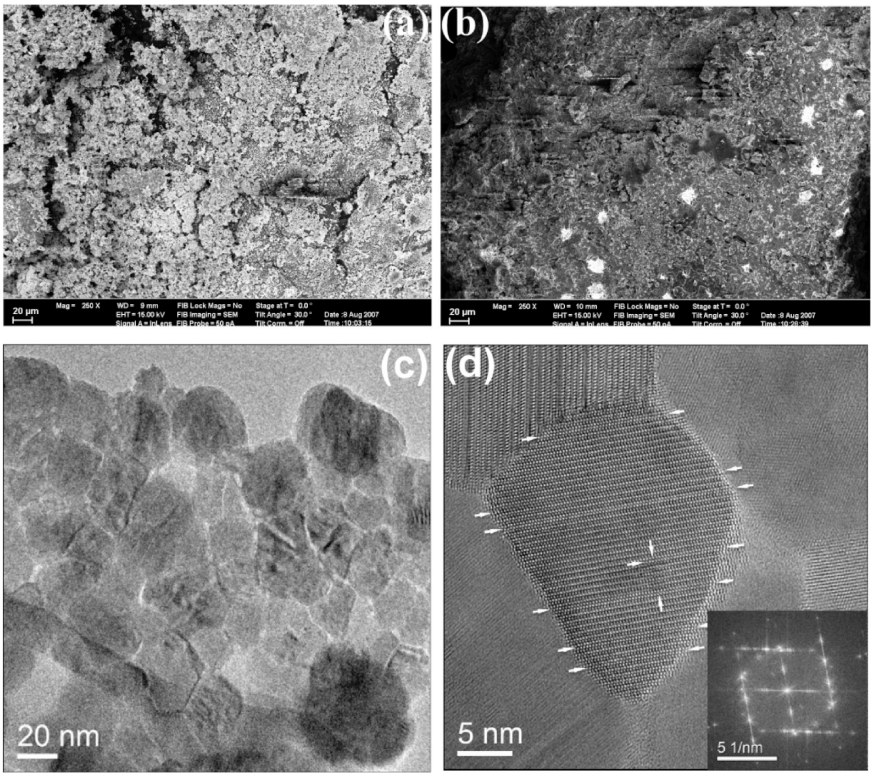

Figure 6. Backscattering electron mode SEM images of the Li-containing ZnO samples with (a) 6% Li and (b) 25% Li. The images of the remaining samples are shown in the Supporting Information. (c) Conventional TEM image and (d) corresponding atomically resolved TEM image with diffractogram of the Li-containing ZnO sample with 1% Li. The small arrows indicate the positions of stacking faults. The TEM images for the samples containing 6% Li and 12% Li, respectively, are shown in the Supporting Information.

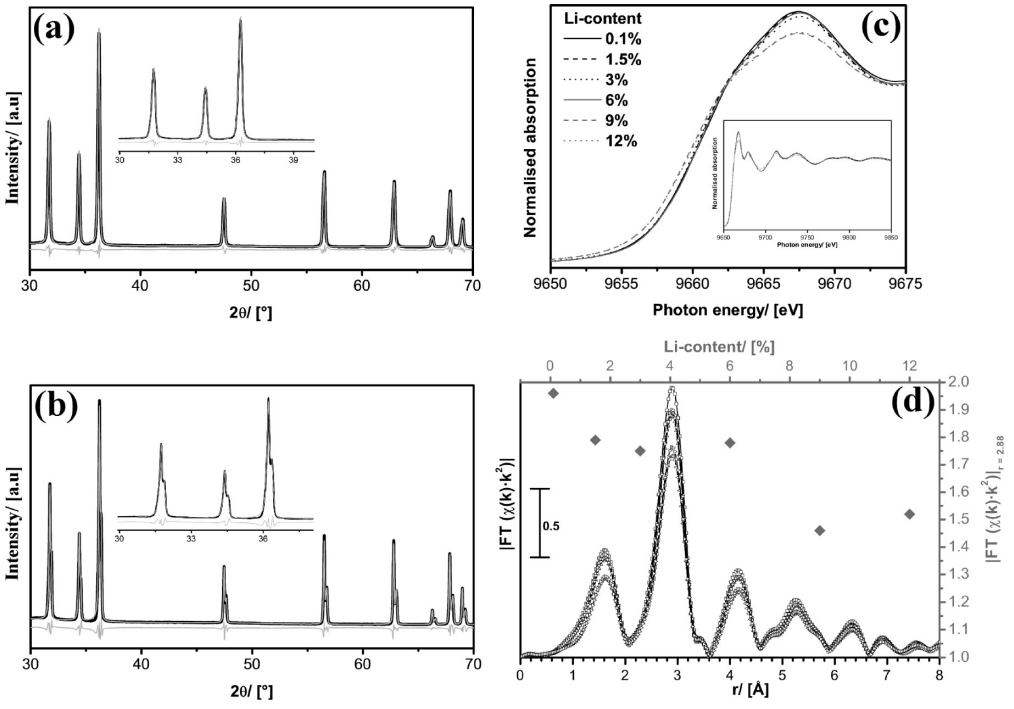

Figure 7. PXRD data of the (a) 3% Li-containing sample and the (b) 12% Li-containing sample. The graphs show the measured curves (black) and the Warren−Averbach fit (gray). The inset is a magnification of the region 30−40° 2θ. The PXRD patterns of the remaining samples are shown in the Supporting Information. (c) XANES and (d) EXAFS recorded at the Zn K-edge for different Li-containing ZnO samples. In (d), the intensity second peak in EXAFS is plotted as a function of Li content (gray).

It is seen in the PXRD pattern of the sample containing 12% Li that all reflexes are split, indicating that two different ZnO phases are present. One of these phases is characterized by a strong expansion of the lattice (a = 327.3 pm; c = 524.3 pm), whereas the remaining phase has similar lattice constants than the ZnO materials

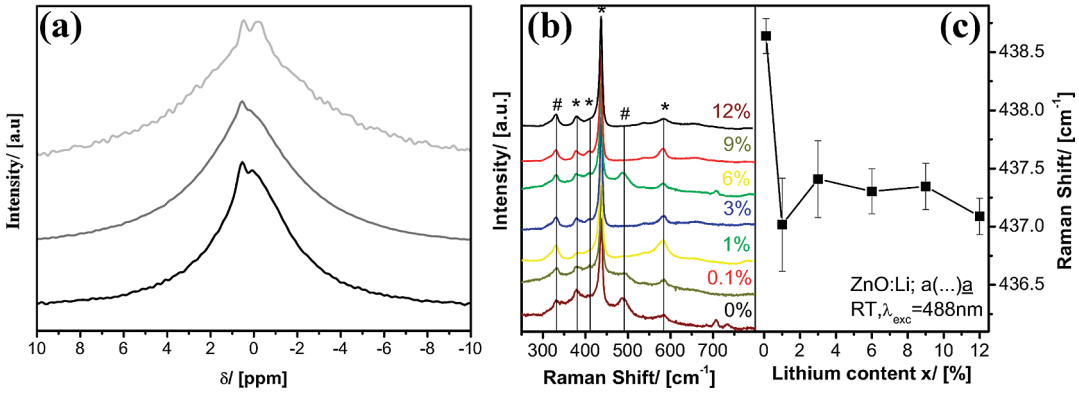

Figure 8. (a) ^{7}Li solid-state NMR spectra of three Li-containing ZnO samples. The spectra for the entire spectral region are shown in the Supporting Information. (b) Raman spectra of undoped (bottom) and lithium-doped ZnO powders with different lithium concentrations. First-order phonon modes are marked with asterisks, second-order phonon modes with hash marks. Spectra are shifted horizontally for better visibility. (c) Raman shift of the E_2(high) mode for different lithium concentrations. Vertical bars mark the standard deviation for the measurements.

containing less Li. The segregation into a new phase can presumably be explained by the factor that above 9% Li more interstitial sites are occupied. Additional information about the structure of the Li containing ZnO materials was acquired by XAS measurements at the Zn−K edge. The edge jump and the whiteline decrease observed in the X-ray absorption near edge structure (XANES) shown in Figure 7c documents the decreasing amount of Zn in the Li-containing samples. In the extended X-ray absorption fine structure (EXAFS) shown in Figure 7d, it is seen that the incorporation of Li effects the zinc coordination. It needs to be emphasized that according to PXRD supported by TEM the particle size of the materials is in the range of 70 nm. Differences in EXAFS can therefore not be assigned to particle size effects. The effects are most pronounced for the peak at r = 4.054 Å associated with the second coordination shell. Because this coordination shell contains zinc atoms as the second-nearest neighbors, it is expected that the substitution of Zn with Li leads to a decrease of the second peak in EXAFS. The latter effect is seen indeed (Figure 7d). ^{7}Li NMR spectra were recorded from three samples and are shown in Figure 8a (overview spectra are shown in the Supporting Information, SI-7). As typical for ^{7}Li solid-state NMR one sees only small differences in chemical shifts and quite broad signals. However, two signals can be identified (δ_1 = 0.5 ppm, δ_2 = −0.02 ppm). The intensity of the signal δ_2 is increasing with increasing Li-content in the samples. Furthermore, the signal δ_2 is broader and is characterized by a longer spin−lattice relaxation time which indicates that the Li correlating to this signal is located in a slightly more asymmetric environment than the Li correlating to δ_1. The solid-state NMR measurements support the previous assumptions that initially most of the Li centers are replacing Zn in the ZnO lattice, but at higher Li contents more and more of the Li is located at undesired, interstitial positions. To obtain information about the vibrational modes and the strain in the samples, we performed micro-Raman spectroscopy. Figure 8b shows the Raman spectra of the Li-doped samples. Additionally, a spectrum of an undoped ZnO powder sample, grown from the precursor "Zn_4O_4" under the same conditions as the doped one, is shown. As expected, all first-order phonon modes (marked by asterisks) are observed.[26] Furthermore, some modes appear that are also visible in pure ZnO and can be clearly identified as second-order modes (hashes).[27] It should be mentioned, that no additional lines appear and no splitting of any of the lines can be seen in any of the spectra, even at high doping levels. This indicates a good incorporation of the Li atoms into the ZnO lattice and in particular on Zn places. The nonpolar E_2(high) mode gives information about the strain in the samples. Figure 6c shows the Raman shift of this mode depending on the doping level. For very low Li concentrations (0.05%) a shift of around 1.6 cm^{-1} from the relaxed value (437 cm^{-1})[27] can be seen, indicating a compressive strain. The situation is different for increased doping levels and leads to nearly relaxed crystals in the case of 12% lithium. The samples show a special behavior in the low doping level regime, as it was observed in PXRD and UV reflection measurements. Thus Li doping in the range of ∼1% seems to be most interesting, because for higher concentrations only small changes in the properties can be observed. The compressive strain in the powders is very striking, since normally ZnO: Li reveals a relaxed E_2(high) or maximal small tensile strain.[29] The vertical bars in Figure 8c mark the standard deviation (SD) for the position of the E_2(high) obtained from different measurement at the samples. On average the SD is around 0.2 cm^{-1}, which, additional to PXRD measurements, indicates a high homogeneity of the nanocrystals.

The band gap energies (E_g, Figure 9a) at room temperature were received from UV/vis measurements acquired in transmission and in diffuse reflectance mode (measurement data shown in SI-8). A local minimum in E_g is seen between 1.5 and 3% Li-content, thus, for similar values for which a maximum in deviation of lattice parameters

(26) Damen, T. C.; Porto, S. P. S.; Tell, B. *Phys. Rev.* **1966**, *142*, 570.
(27) Calleja, J. M.; Cardona, M. *Phys. Rev. B* **1977**, *16*, 3753.
(28) Bundesmann, C.; Ashkenov, N.; Schubert, M.; Spemann, D.; Butz, T.; Kaidashev, E. M.; Lorenz, M.; Grundmann, M. *Appl. Phys. Lett.* **2003**, *83*, 1974.
(29) Sakai, A.; Islam, E.; Aoki, T.; Onodera, A. *Ferroelectrics* **2000**, *239*, 1003.

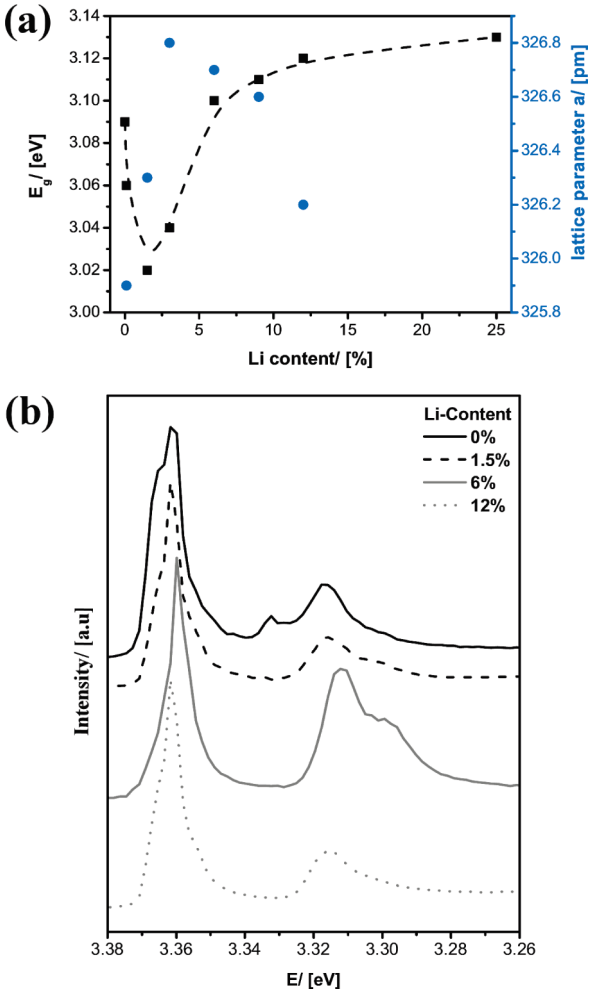

Figure 9. (a) Lattice parameter *a* (blue circles) and the band gap energy (black squares) as a function of the Li content. (b) Low-temperature photoluminescence spectra of three Li containing ZnO materials and pure ZnO (prepared from "Zn_4O_4") as a reference. All spectra are normalized to the intensity of the excitonic emission at 3.36 eV. The entire PL spectra recorded between 1.5 and 3.5 eV are shown in the Supporting Information.

has been observed in PXRD (Figure 7a). This finding is in good agreement with other papers which have reported that 0.8 at % Li in ZnO is special since a maximum change in opto-electrical properties has been observed.[13,14] Further information about the properties of the Li containing ZnO materials was acquired from low-temperature photoluminescence (PL) measurements (Figure 9b). The luminescence spectra are dominated by a strong emission at 3.36 eV, which originates from the recombination of bound excitons. The full width at half-maximum (fwhm) of the excitonic luminescence is as sharp as 1 meV, which indicates a high sample quality. Remarkably, the excitonic luminescence shows a narrow line width and high intensity even for the highest Li content. In addition, a strong luminescence at 3.31 eV is observed, which is related to surface defects.[24] This luminescence is common for ZnO nanostructures and can vary in intensity with the crystal size. With increasing Li concentration a peak at 3.23 eV becomes visible, followed by its first longitudinal-optical (LO) phonon replica at 3.16 eV. We attribute this luminescence to a donor−acceptor pair

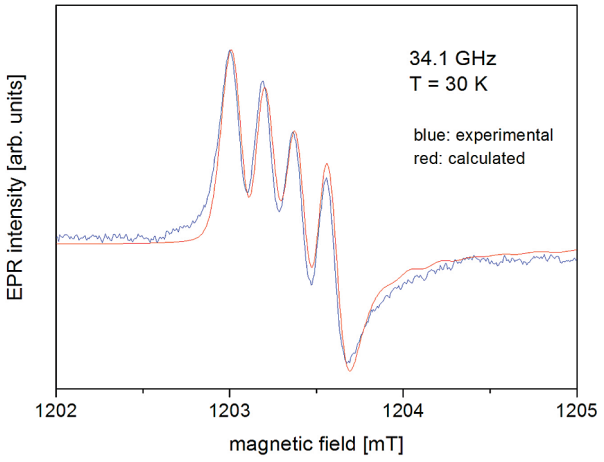

Figure 10. Resolved hyperfine structure of the EPR spectrum (low-magnetic field site) of the axial Li^+-O^- defects for nanocrystalline ZnO in the Q-band at $T = 30$ K. The experimental HF-structure was observed for a ZnO nanocrystals ensemble with nominal 1% Li 10 min after terminating its illumination with laser light of 442 nm to reduce strongly the contribution of the overlapping HF structure caused by the nonaxial Li^+-O^- defects.[31] The calculated structure was obtained using the SH parameter for Li on Zn site in ZnO crystals.[30a].

luminescence (DAP) involving an acceptor with a binding energy of about $E_A = 150$ meV, which is associated with the incorporation of Li.[25,31] In the spectral region below 2.5 eV, a green luminescence band is observed (see the Supporting Information, SI-9), which is caused by intrinsic defects. The low intensity of this defect luminescence in comparison to the excitonic luminescence further demonstrates the good quality of the samples.

The incorporation of Li in the ZnO lattice was also studied by electron-paramagnetic resonance spectroscopy (EPR). For samples not doped with Li we found only the shallow donor signal at $g = 1.956$ and weak signals from $Mn_{Zn}{}^{2+}$.[30b,c] The Li-doped samples exhibit in addition to the Mn^{2+} signals also the EPR spectrum of Fe^{3+} on Zn site but without illumination no any longer the shallow donor signal and no indication of any Li acceptor signals.[31] However, under illumination with laser light of 325 nm and/or 442 nm below 200 K, the shallow donor signal was detected again and in addition the characteristic spectrum of the Li_{Zn} acceptor is observed.[31] These results indicate that the shallow donor signal disappeared only by recharging of the shallow donor owing to a shift of the Fermi level in direction to the valence band but without reaching the energy level position of the $Li_{Zn}{}^+-O^{2-}$ defect to the paramagnetic state $Li_{Zn}{}^+-O^-$. The experimental results concerning the paramagnetic Li acceptors were compared with simulations of the powderlike spectra using the SH parameter obtained for Li on Zn site in hexagonal ZnO single crystals[30a] and taken into account the different orientation of the axial

(30) (a) Schirmer, O. F. *J. Phys. Chem. Solids* **1968**, *29*, 1407. (b) Meyer, B. K.; Alves, H.; Hofmann, D. M.; Kriegseis, W.; Forster, D.; Bertram, F.; Christen, J.; Hoffmann, A.; Strassburg, M.; Dworzak, M.; Haboeck; Rodina, U., A. V. *Phys. Stat. Sol. B* **2004**, *241*, 231. (c) Vlasenko, L.; Watkins, G. *Phys. Rev. B* **2005**, *72*, 35203.
(31) Rauch, C., Gehlhoff, W., Wagner, M. R., Malguth, E., Callsen, G., Kirste, R., Salameh, B., Hoffmann, A., Aksu, Y., Driess, M., Polarz, S. **2009**, submitted.

and nonaxial Li^+-O^- defects in hexagonal ZnO nanocrystals with random distribution of the crystal axes.[31] The perfect agreement between the complete experimental and calculated spectra as well as the resolved hyperfine splitting caused by the ^7Li isotope with a nuclear spin $I = 3/2$ shown in Figure 10 for the axial centers clearly proves that the observed Li defect occupies like in single crystals on the Zn site.[31]

4. Conclusion

A new, organometallic precursor system was introduced in this study which allowed the preparation of alkali-metal-doped and in particular Li-doped zinc oxide materials with various Li contents. It was found that between 12 and 25% Li content the Li is not stable in the ZnO matrix and the formation of an additional, amorphous carbonate phase can be observed. Below 9%, Li a significant amount of the dopant substitutes Zn in the ZnO lattice. Between 9 and 12% Li, more and more Li is located at interstitial positions, which finally leads to a phase separation of two distinguishable Li−ZnO phases. Even in the range 0−9%, the properties of the Li-containing ZnO materials do not scale continuously with the amount of Li incorporated. Materials in the range 1−3% Li appear to be special structurally and electronically, most importantly regarding the p-character of the ZnO material.

Acknowledgment. We thank the Grillo-group and Grillo Zinkoxid GmbH for financial support. The Deutsche Forschungsgemeinschaft is acknowledged for funding (project PO780/4-1, DR 226/16-1 and SFB 787). We thank Dr. M. Merz and S. Schütte for help during the synthesis of the molecular precursors, and Dr. K. Merz for performing the single-crystal X-ray analysis. The possibility and support for using the spherical aberration corrected FEI Tecnai F20 TEM in the workgroup of Prof. Hannes Lichte at the Triebenberg Lab of the TU Dresden is gratefully acknowledged.

Supporting Information Available: SI-1, additional analytical data for compound $[Me_3Zn_3Na(thf)OtertBu_4]$; SI-2: sublimation of "$Zn_3LiO_4$"; SI-3, TGA trace of the decomposition of precursor "Zn_3LiO_4" under pure oxygen; SI-4, SEM images of prepared Li containing ZnO materials; SI-5, TEM images of prepared Li-containing ZnO materials; SI-6, overview over PXRD data acquired from the Li-containing ZnO samples; SI-7, ^7Li solid-state spectra (overview); SI-8, optical spectra; SI-9, photoluminescence spectra (PDF). This material is available free of charge via the Internet at http://pubs.acs.org.